1-4-91
E5912

NASA Technical Memorandum 103693

Icing Characteristic of a Natural-Laminar-Flow, a Medium-Speed, and a Swept, Medium-Speed Airfoil

Colin S. Bidwell
Lewis Research Center
Cleveland, Ohio

Prepared for the
29th Aerospace Sciences Meeting
sponsored by the American Institute of Aeronautics and Astronautics
Reno, Nevada, January 7–10, 1991

NASA

ICING CHARACTERISTICS OF A NATURAL-LAMINAR-FLOW, A MEDIUM-SPEED, AND A SWEPT, MEDIUM-SPEED AIRFOIL

Colin S. Bidwell
National Aeronautics and Space Administration
Lewis Research Center
Cleveland, Ohio 44135

Summary

Tests were conducted in the Icing Research Tunnel at the NASA Lewis Research Center to determine the icing characteristics of three modern airfoils, a natural-laminar-flow, a medium-speed and a swept, medium-speed airfoil. The tests measured the impingement characteristics and drag degradation for angles-of-attack typifying cruise and climb for cloud conditions typifying the range that might be encountered in flight. The maximum degradation occurred at the cruise angle-of-attack for the long, glaze ice condition for all three airfoils with increases over baseline drag being 486%, 510%, and 465% for the natural-laminar-flow, the medium-speed and the swept, medium-speed airfoil respectively. For the climb angle-of-attack the maximum drag degradation (and total extent of impingement) observed were also for the long, glaze ice condition and were 261%, 181% and 331% respectively. The minimum drag degradation (and extent of impingement) occurred for the cruise condition and for the short, rime spray with increases over baseline drag values being 47%, 28%, 46% respectively.

Nomenclature

C_d	Wing section drag coefficient.
C	Wing chord, feet.
LWC	Icing cloud liquid water content, gm/m^3.
M	Free stream Mach number.

MVD	Median volume water droplet diameter, microns.
Re	Reynolds number.
TO	Total temperature, ° F.
X	Airfoil axial coordinate, feet.
Y	Airfoil normal coordinate, feet.
V	Free stream velocity, mph.
α	Wing section angle-of-attack in wind tunnel measurement plane, degrees.
τ	Icing spray time, minutes.

Introduction

As part of the icing research program at NASA Lewis Research Center a series of tests to determine the icing characteristics of several modern airfoils was conducted. The airfoils included a natural-laminar-flow (NLF(1)-0414), a medium-speed (MS(1)-317) and a swept, medium-speed airfoil (MS(1)-317 with 30 degrees of sweep). The icing characteristics measured included section drag, ice shape tracings and impingement efficiency. These tests, which involved several entries in the NASA Lewis Icing Research Tunnel (IRT) over a period of seven years beginning in 1983, were the first such tests for these airfoils.

The natural-laminar-flow (NLF) airfoil was designed in the early 1980s as a medium-speed airfoil with low section drag and high maximum section lift (Ref. 1). The NLF(1)-0414 tested was designed for 0.70C laminar flow on both surfaces, a lift coefficient of 0.4, a Reynolds number of 10.0 x 10^6, and a Mach number of 0.4.

The MS(1)-317 airfoil was designed in the mid 1970s to bridge the gap between the low-speed and supercritical airfoils for application on general aviation aircraft (Ref. 2). The airfoil was designed for a lift coefficient of 0.3, an Reynolds number of 14.0 x 10^6, and a Mach number of 0.68.

Experimental Apparatus

The ice accretion and impingement efficiency tests were carried out in the NASA Lewis IRT (figure 1). The test equipment included the three models, drag wake survey system, molding compounds for making ice accretion molds, a 35 mm camera and cardboard templates for documenting ice shape, a special spray system for the impingement tests (ref. 3,4), a laser reflectometer for impingement efficiency data reduction, and the ESCORT data analysis system for recording and calculating other pertinent test information.

The IRT facility can provide a range of airspeeds, angle of attacks, temperature, liquid water contents (LWC), and drop sizes (ref. 5). The IRT has a 9 ft x 6 ft test section with a maximum airspeed of 300 mph (empty tunnel). Angle-of-attack is controlled by a movable turntable to which the models are mounted. A refrigeration system allows year-round testing of temperatures from -20° F to 50° F. The spray system located upstream of the test section can provide a cloud with an LWC of 0.25 - 3.0 g/m^3 and a median volume drop (MVD) size range of 14 - 40 μm.

The NLF(1)-0414 model (figure 2) was constructed for the IRT test section. The model was made of mahogany with a fiberglass trailing edge and had a 6 foot span and a 3 foot chord. Coordinates for the section are given in table I.

The MS(1)-317 models were also constructed for the IRT test section. Both models were full span (6 foot span) and had three foot chords. The straight MS(1)-317 model shown in figure 3 was of fiberglass construction and contained 50 static pressure taps at the mid-span position. The swept MS(1)-317 (figure 4) was made of mahogany and had a 30 degree sweep angle. The swept airfoil was unusual in that the MS(1)-317 coordinates were constructed in the free stream flow direction and that the trailing edge was closed. This unusual design was thicker than the usual swept MS(1)-317 constructed in the leading edge normal direction. The coordinates for the MS(1)-317 section are given in table II.

A drag wake survey probe was used to measure total pressure profiles in the wake behind the airfoils. These pressure profiles were then used to calculate the section drag of the airfoil. The drag wake probe consisted of a pitot probe mounted on a track which allowed the probe to traverse across the airfoil wake at the midspan of the airfoil. Figure 2 shows the wake survey system installed behind the NLF(1)-0414 airfoil.

The Escort system was developed at Lewis to aid in storage, processing, and analysis of large amounts of data (e.g. temperature, pressure) produced in various experiments at the Center. In this test Escort was used to store tunnel total temperature, total pressure, free stream airspeed and wake total pressures, produce on-line calculations and display pertinent parameters. The storage sequence for each data point was initiated by the researcher in the control room. Escort then assigned a reading number to this stored data for cataloging purposes. A separate program was used to do a more complete post run analysis. This analysis included plotting wake profiles and calculating drag.

The spray requirements for the impingement tests precipitated the need for a different spray system than was available in the IRT (ref. 3). The IRT spray system could not produce the short (1-3 seconds), stable sprays (i.e. constant LWC and drop size) required to prevent blotter strip saturation. There were also concerns that the dye would contaminate the IRT spray system. The new spray system consisted of 12 nozzles and a supply tank located at the IRT spray bar station (figure 5). The system featured short supply lines which enabled short, stable sprays.

Experimental Procedure

Two types of testing were done in the IRT for the airfoils: ice accretion and impingement efficiency testing. The ice accretion testing involved taking drag data, ice shape tracings, and photographs for various icing conditions. The impingement efficiency testing involved the use of a dye tracer technique to measure the location and amount of water striking the model.

The airfoil section drag was calculated from total pressure profiles measured with the wake survey probe. The data was corrected for probe and model blockage. The method for reducing the data is outlined in reference 6. Clean airfoil drag coefficient repeatability has been measured in the past, with ± 8% deviation from the average value at one standard deviation (ref. 7).

A total of 92 icing sprays were made. These sprays are summarized in tables III, IV and V for each of the airfoils . The total temperatures for the icing runs were chosen to span the range of ice accretions from rime to glaze. The 0° F conditions produced typical rime ice accretions while the 15° F and 28° F conditions produced mixed and glaze conditions respectively. Two angles of attack were chosen for each of the airfoils to typify cruise and climb configurations. Because of tunnel and model limitations, typical flight speeds for the wing sections could not be attained. In general, 150 mph was used for most of the model tests. In an attempt to produce meaningful results for use in flight analysis the drop size and the LWC for the tests were loosely scaled to account for the velocity deficiency. This scaling resulted in larger drop sizes and LWC than typically encountered in flight. A number of spray durations were chosen to shed light on the time dependence of the drag degradation. For all cases, drag performance was measured for the same angle of attack at which the ice was accreted. In addition performance data was taken for several of the ice accretions at angles-of-attack other than those at which the ice was accreted.

The experimental technique used in the current tests to determine the impingement characteristics of a body is one that was developed in the early 1950s with a few modifications (ref. 3,4). The technique involved spraying a dye-water solution of a known concentration onto a model covered with blotter strips. Figure 3 shows a typical blotter installation for the MS(1)-317 airfoil. The result being that the local impingement efficiency rate is reflected on the blotter strips as a variation in color intensity. That is, the areas of higher impingement rate are darker and those with lower impingement rate are lighter. One unique feature of the current technique is the laser reflectometer used to determine the local collection efficiency (figure 6). The device measures the local reflectance of the blotter strip and correlates this to the local collection efficiency. The device saved considerable time in the data reduction of the blotter strips.

Several steps were necessary to prepare the IRT for impingement testing. The specially designed spray system had to be installed and adjusted to produce a uniform cloud. The local LWC had to be measured at each blotter strip location (with the tunnel empty) every spray and tunnel condition to account for any cloud nonuniformity that existed after the final spray adjustment. After these adjustments and measurements were made the model was inserted and tested. Each point was repeated five times to obtain a statistical average.

A typical run for an airfoil involved several steps. The model was cleaned and blotter strips were attached at points of interest (figure 3). The spray was then made, the blotter strips were removed, and labeled, and the model was cleaned and made ready for the next condition.

Table VI summarizes the test matrix for the impingement tests. All of the models were tested for two drop sizes and at two angles-of-attack. The angles of attack were chosen to simulate a cruise and a climb configuration. Two medium volume diameter sizes were chosen to typify those that might be encountered in flight.

Analysis

Two types of data were analyzed: airfoil drag and impingement efficiency. A discussion of the quality of the clean airfoil drag will be followed by a discussion of the iced airfoil drag performance and by a discussion of the impingement characteristics of the airfoils. The drag performance analysis will be divided into four parts: temperature effects, spray length effects, drop size effects, and off-condition effects (performance of iced airfoil at angles-of-attack other than those for which the ice was accreted). The impingement analysis will be divided into two parts: angle of attack and drop size effects.

Figures 7-9 show the clean airfoil drag performance. Superimposed on the data are results from previous tests of the airfoils at the NASA Langley Low Turbulence Pressure Tunnel (LTPT) given in references 1 and 2. At the higher angles-of-attack the IRT data compares well with the LTPT data with the IRT producing slightly lower drag values. This difference is probably due to the blockage correction made in the IRT data (ref. 6). At the lower angles-of-attack the IRT data falls somewhere between the rough and smooth configuration data from the Langley tests. This result is typical for IRT tests and occurs for several reasons; differences in wake measurement, tunnel turbulence levels and model surface conditions. The Langley tests used a wake rake while the IRT tests used a traversing probe. Turbulence intensity levels in the IRT are typically 0.5 % while those for the LTPT are typically 0.1 % (ref. 8). The IRT models finish, although comparable to those of the Langley models initially, deteriorated with each deicing cycle.

Figures 10-12 summarize the temperature dependence of the drag coefficients for the three airfoils at various angles-of-attack. Figure 11, which shows this temperature dependence in the highest resolution, is typical (ref. 6,7,9). The drag degradation is a minimum above freezing (clean condition), it increases sharply to a maximum around 31° F (glaze condition), drops off rather rapidly to 15° F (mixed condition), and flattens out with an approximately constant value at 5° F (rime). Noteworthy in Table IV is the scatter in the drag data around the peak at 31 degrees. This scatter is probably due to the high sensitivity of ice shape to temperature in the glaze regime and the fact that the IRT temperature control is not exact. That is, target temperature drift throughout a spray and temperature profile variability between sprays can occur, and even a small variation in total temperature (± 1° F) can cause a significant difference in the ice accretion and its associated drag.

Drag performance as a function of spray time for the three airfoils is summarized in figures 13-15. All three airfoils exhibited an increase in drag coefficient with time in an almost linear fashion at a given temperature. As temperature was increased toward the freezing point the slope of the drag degradation versus icing time curve increased. This linear increase in drag with time is a typical result (ref. 6,7,9).

Figure 16 shows, the effect of drop size on the drag coefficient for the MS(1)-317 airfoil in the glaze regime. The figure shows an almost linear relationship between drag coefficient and drop size, with the largest drop size (20 μm) producing the largest drag increase (500 %). This trend is reasonable considering the limited drop size range tested and is similar to that exhibited by the correlation of Gray (Ref. 9).

For several of the ice accretions, drag performance as a function of angle-of-attack was explored. These cases are useful in evaluating the ability of the planform to maneuver with a given ice accretion. Figures 17 and 18 show the drag polars for these cases while photographs and tracings of these accretions are shown in figures 19-21. Several features are noteworthy and are typical (ref. 6,7,9). The first being that in the glaze regime the drag penalties at a given angle-of-attack are higher for the cruise than for the climb icing angle-of-attack for the same icing conditions. This result can be explained when we examine the aerodynamics of the ice accretions generated at the cruise and climb angles-of-attack for the same icing condition. In general the ice accretion generated at the lower angle-of-attack will have a larger protuberance on the suction side of the airfoil than for that generated at the higher angle-of-attack. This upper surface protuberance produces a spoiler effect and is one of the main contributors to the drag degradation. Hence, the ice accretion at the lower angle of attack will have the larger penalty at a given angle-of-attack. Another feature shown in figure 18a for the long, rime, spray is the occurrence of the minimum drag coefficient at the iced angle-of-attack. This result is common for long, rime, sprays. This feature can also be explained when we examine the physics of the ice accretion. Because of the thermodynamics (i.e. the drops freeze upon impact) and the aerodynamics (i.e. the drops follow the streamlines) the rime accretion grows in the flow direction. This alignment of the ice shape with the flow produces a camber or leading edge flap effect. And as for a cambered wing or a wing with a leading edge flap, the drag of the ice shape is increased at off design angle-of-attacks (i.e. other than when the leading edge is aligned with the flow).

Table VII summarizes the percent drag degradation for various cases of interest. These cases yielded the maximum and minimum percent drag degradation with respect to temperature, icing time, angle-of-attack, and temperature for each of the airfoils.

Two parameters were explored for the three models in the impingement tests: angle-of-attack and drop size. Figure 23 summarizes the results of the tests. Several features are typically examined when analyzing impingement efficiency for an airfoil: maximum collection efficiency, impingement limits or total extent of impingement (i.e. surface distance between upper and lower impingement limits) and the total collection efficiency (i.e. the total amount of water collected). In general, at a given angle-of-attack the smaller drop size (16 μm) produced smaller maximum impingement efficiency, extent of impingement and total collection efficiency. This is because the smaller droplets have smaller inertia and are more apt to follow the streamlines, hence missing the body. Also, in general, for a given drop size the cruise configuration produced a higher maximum impingement efficiency, a smaller total extent of impingement and a smaller total collection efficiency than the climb configuration.

Summary of Results

The icing and impingement characteristics of the three airfoils were studied for conditions typifying cruise and climb in the NASA Lewis Icing Research Tunnel. Drag coefficient measurements, photographs, and tracings of ice shapes were made for the ice accretion tests. Measurements of local impingement efficiency were made during the dye tracer tests.

The impacts of icing temperature, icing spray time, and drop size on the performance of the iced airfoils for several flight configurations were explored during the test. In general, icing temperature had a nonlinear effect on airfoil performance degradation, with performance degradation being a minimum at the colder temperatures (0° F), increasing in a nonlinear fashion to near freezing, and falling off rapidly to the clean value at the freezing point. And, in general, icing time had a linear effect on iced performance degradation, with performance degradation being a minimum for the clean configuration. For the drop size range tested drop size had a linear effect on performance degradation, with performance degradation being a minimum for smallest drop size.

For the cruise angles-of-attack the maximum penalties occurred for the longest duration, highest LWC sprays tested for all three airfoils. The glaze condition produced the absolute maximum drag degradation for all three airfoils. The performance losses for this worst case were 486%, 510%, and 465% for the NLF(1)-0414, MS(1)-317, and swept MS(1)-317 airfoils, respectively. For the longest duration, rime sprays the performance losses were 83%, 68%, and 58% for the airfoils, respectively.

For the climb angles-of-attack the longest duration, highest LWC sprays also produced the maximum drag degradation for all three airfoils. The glaze condition yielded performance losses of 261%, 181% and 331% for the NLF(1)-0414, MS(1)-317, and swept MS(1)-317 airfoils, respectively. For the longest duration, rime sprays the performance losses were 74%, and 122% for the NLF(1)-0414 and swept MS(1)-317 airfoils, respectively.

For the cruise condition (angle-of-attack, 0°; airspeed, 150 mph) the largest maximum impingement efficiency, total extent of impingement and total collection efficiency occurred for the largest medium volume diameter spray (20 μm). The largest maximum impingement efficiencies for the NLF(1)-0414, the MS(1)-317 and the swept MS(1)-317 were 43%, 48%, and 58% respectively. The maximum total extent of impingement (% of chord) were 9%, 17%, and 17% for the airfoils respectively.

For the climb condition (angle-of-attack, 8°; airspeed, 150 mph) the largest maximum impingement efficiency, total extent of impingement and total collection efficiency also occurred for the largest medium volume diameter spray (20 μm). The largest maximum impingement efficiencies for the NLF(1)-0414, the MS(1)-317 and the swept MS(1)-317 were 62%, 48%, and 64% respectively. The maximum total extent (% of chord) of impingement were 18%, 26%, and 25% for the airfoils respectively.

References

1. McGhee, R.J., Viken, J.K., Pfenninger, W., Beasley, W.D., and Harvey, W.D., "Experimental Results For a Flapped Natural-Laminar-Flow Airfoil" NASA TM 85788, 1984.

2. McGhee, R.J., Beasley, W.D., "Low-Speed Aerodynamic Characteristics of a 17-Percent-Thick Medium-Speed Airfoil Designed for General Aviation Application" NASA TP 1786, 1980.

3. Papadakis, M., Elangonan, G.A., Fruend, G.A.,Jr., Breer, M., Whitmer, L., "An Experimental Method for Measuring Water Droplet Impingement Efficiency on Two- and Three-Dimensional Bodies", NASA CR 4257, DOT/FAA/CT-87/22.

4. Papadakis, M., Beer, M.D., Craig, N.C., Bidwell, C.S., "Experimental Water Droplet Impingement Data on Modern Aircraft Surfaces",AIAA-91-0445, 1991.

5. Soeder, R.H., Andracchio, C. R., "NASA Lewis Icing Research Center Tunnel User Manual", NASA TM 102319, 1990.

6. Shaw, R.J., Sotos, R.G., "An Experimental Study of Airfoil Icing Characteristics", NASA TM 82790, 1982.

7. Olsen, W., Shaw, R.J., Newton, J.E., "Ice Shapes and the Resulting Drag Increase for a NACA 0012 Airfoil", NASA TM 83556, 1982.

8. von Doenhoff, A.E., Abbot, A.E., "The Langley Two-Dimensional Low-Turbulence Pressure Tunnel", NACA TN 1283, 1947.

9. Gray, V.H., "Predictions of Aerodynamic Penalties Caused by Ice Formations on Various Airfoils", NASA TN D-2166, 1964.

TABLE I. - NLF(1)-0414 AIRFOIL COORDINATES.

UPPER SURFACE

X/C	Y/C	X/C	Y/C	X/C	Y/C
.000000	.000000	.245187	.074349	.735392	.047492
.000085	.001585	.261054	.075830	.750058	.042542
.000299	.003274	.277233	.077161	.764925	.037208
.001231	.007144	.293699	.078380	.779951	.031694
.002695	.010618	.310424	.079454	.795034	.026178
.004989	.014163	.327391	.080369	.810124	.020750
.008005	.017552	.344571	.081151	.825179	.015483
.011774	.020769	.361925	.081781	.840076	.010464
.016268	.023816	.379421	.082240	.854693	.005783
.021468	.026795	.397052	.082536	.868960	.001467
.027356	.029735	.414812	.082677	.882768	-.002475
.033891	.032633	.432667	.082633	.896006	-.006044
.041042	.035480	.450558	.082429	.908644	-.009267
.048811	.038317	.468450	.082047	.920659	-.012161
.057201	.041092	.486327	.081507	.931980	-.014739
.066189	.043825	.504159	.080794	.942511	-.017008
.075767	.046482	.521931	.079893	.952200	-.018994
.085915	.049070	.539641	.078779	.961042	-.020722
.096610	.051588	.557254	.077489	.969034	-.022206
.107826	.054033	.574742	.075988	.976155	-.023456
.119545	.056398	.592064	.074285	.982370	-.024492
.131756	.058692	.609177	.072377	.987660	-.025333
.144443	.060917	.626040	.070245	.992021	-.026006
.157592	.063092	.642629	.067900	.995456	-.026519
.171193	.065206	.658928	.065348	.997952	-.026872
.185212	.067240	.674926	.062510	.999480	-.027067
.199628	.069172	.690586	.059376	1.000000	-.027122
.214447	.071009	.705860	.055889		
.229647	.072735	.720751	.055194		

TABLE I. - CONTINUED. NLF(1)-0414 AIRFOIL COORDINATES.

LOWER SURFACE

X/C	Y/C
.000000	.000000
.000085	-.001535
.000164	-.002120
.000740	-.004536
.002095	-.006984
.004175	-.009008
.007129	-.010993
.010874	-.012933
.015540	-.014882
.021096	-.016854
.027380	-.018787
.034569	-.020742
.042393	-.022654
.050985	-.024572
.060274	-.026487
.070243	-.028383
.080881	-.030259
.092159	-.032116
.104058	-.033945
.116557	-.035741
.129635	-.037497
.143277	-.039212
.157457	-.040888
.172148	-.042421
.187328	-.044107
.202969	-.045646
.219043	-.047125

X/C	Y/C
.235525	-.048542
.252387	-.049901
.269586	-.051189
.287087	-.052411
.304866	-.053561
.322901	-.054635
.341156	-.055635
.359611	-.056539
.378260	-.057344
.397074	-.058052
.416017	-.058658
.435049	-.059142
.454127	-.059517
.473222	-.059785
.492319	-.059950
.511402	-.060012
.530430	-.059979
.549361	-.059792
.568160	-.059456
.586782	-.058982
.605204	-.058340
.623397	-.057533
.641303	-.056524
.658920	-.055246
.676262	-.053698
.693229	-.051845
.709795	-.049388

X/C	Y/C
.726433	-.046065
.743743	-.042296
.761642	-.038850
.779550	-.035991
.797188	-.033529
.814513	-.031444
.831368	-.029735
.847719	-.028310
.863493	-.027230
.878523	-.026450
.892802	-.025925
.906336	-.025641
.919043	-.025539
.930841	-.025569
.941715	-.025689
.951668	-.025861
.960696	-.026061
.968804	-.026275
.975996	-.026483
.982266	-.026675
.987613	-.026858
.992033	-.027036
.995503	-.027211
.997994	-.027367
.999497	-.027475
1.000000	-.027514

TABLE II. - MS(1)-317 COORDINATES

X/C	Y/C UPPER	Y/C LOWER
.00000	.00099	.00099
.00200	.01248	-.00857
.00500	.01950	-.01366
.01250	.03099	-.02105
.02500	.04322	-.02866
.03750	.05210	-.03423
.05000	.05893	-.03865
.07500	.06840	-.04541
.10000	.07511	-.05058
.12500	.08033	-.05477
.15000	.08454	-.05817
.17500	.08805	-.06099
.20000	.09096	-.06330
.22500	.09339	-.06527
.25000	.09536	-.06685
.27500	.09694	-.06812
.30000	.09815	-.06909
.32500	.09901	-.06978
.35000	.09952	-.07021
.37500	.09972	-.07036
.40000	.09956	-.07019
.42500	.09909	-.06967
.45000	.09826	-.06880
.47500	.09700	-.06755

X/C	Y/C UPPER	Y/C LOWER
.50000	.09535	-.06591
.52500	.09323	-.06389
.55000	.09073	-.06138
.57500	.08777	-.05845
.60000	.08448	-.05501
.62500	.08079	-.05106
.65000	.07672	-.04674
.67500	.07232	-.04214
.70000	.06763	-.03735
.72500	.06269	-.03255
.75000	.05755	-.02780
.77500	.05225	-.02309
.80000	.04687	-.01857
.82500	.04132	-.01433
.85000	.03576	-.01049
.87500	.03013	-.00719
.90000	.02444	-.00460
.92500	.01873	-.00289
.95000	.01302	-.00232
.97500	.00720	-.00324
1.00000	.00125	-.00597

TABLE III. - NLF(1)-0414 ICING SPRAYS

α	V (mph)	TO (°F)	τ (min.)	LWC (g/m^3)	MVD (μm)	C_d
0	150	28	5.	1.0	20.5	.01739
6	150	28	5.	1.0	20.5	.02771
0	150	15	5.	1.0	20.5	.01275
6	150	15	5.	1.0	20.5	.01585
6	150	15	15.	1.0	20.5	.02805
0	150	15	15.	1.0	20.5	.01760
0	150	15	15.	.75	13.5	.01562
0	150	28	6.3	.75	13.5	.01471
0	150	28	18.8	.75	13.5	.01611
0	150	0	5.	1.0	20.5	.01247
6	150	0	5.	1.0	20.5	.02320
*6	150	0	15.	1.0	20.5	.02755
*0	150	0	15.	1.0	20.5	.01546
*,**0	150	0	15.	1.0	20.5	.01622
*6	150	28	15.	1.0	20.5	.05727
*0	150	28	15.	1.0	20.5	.04940
*,**0	150	28	15.	1.0	20.5	.05810

* Drag coefficients obtained for ice accretion at several angles of attack.
** Repeat. Ice shape mold taken.

TABLE IV. - CONCLUDED. MS(1)-317 AIRFOIL ICING SPRAYS.

α	V (mph)	TO (°F)	τ (min.)	LWC (g/m^3)	MVD (μm)	C_d
*2	150	28	15.0	1.3	15.0	.0472
*2	150	25	15.0	1.3	15.0	.0434
*2	150	20	15.0	1.3	15.0	.0242
*2	150	15	15.0	1.3	15.0	.0231
*,**2	150	10	15.0	1.3	15.0	-
2	150	5	15.0	1.3	15.0	.0212
2	150	32	15.0	1.3	15.0	.0236
*2	150	30	15.0	1.3	15.0	.0595
2	150	27	15.0	1.3	15.0	.0451
*,**2	150	25	15.0	1.3	15.0	-
*,**2	150	20	15.0	1.3	15.0	-
*2	150	25	15.0	1.3	15.0	.0532
*2	150	25	15.0	1.3	13.8	.0239
*2	150	25	15.0	1.3	15.0	.0347
*2	150	25	15.0	1.3	17.0	.0504
*2	150	25	15.0	1.3	20.0	.0728
*2	150	25	15.0	1.8	20.0	.0675
*2	150	20	15.0	1.3	15.0	.0300
*2	150	25	15.0	1.3	15.0	.0306
4	150	25	15.0	1.3	15.0	.0297
6	150	25	15.0	1.3	15.0	.0394
8	150	25	15.0	1.3	15.0	.0374
*2	150	31	15.0	1.3	15.0	.0488
*2	150	25	15.0	1.3	15.0	.0379
2	200	25	5.0	1.3	15.0	.0273
2	200	25	10.0	1.3	15.0	.0532
*2	150	25	15.0	1.3	15.0	.0546
2	150	5	5.0	1.3	15.0	.0153
2	150	5	10.0	1.3	15.0	.0169

* Repeat run.

** Missing or bad drag data.

TABLE IV. - MS(1)-317 AIRFOIL ICING SPRAYS.

α	V (mph)	TO (°F)	τ (min.)	LWC (g/m^3)	MVD (μm)	C_d
2	150	30	10.0	1.3	15.0	.0312
2	150	30	5.0	1.3	15.0	.0344
2	150	30	15.0	1.3	15.0	.0414
2	150	25	15.0	1.3	15.0	.0511
2	150	25	10.0	1.3	15.0	.0351
2	150	25	5.0	1.3	15.0	.0240
2	150	25	2.0	1.3	15.0	.0147
2	150	20	15.0	1.3	15.0	.0276
2	150	25	15.0	1.3	20.0	.0624
2	150	25	15.0	1.8	20.0	.0794
2	150	25	15.0	1.3	13.8	.0544
2	150	15	15.0	1.3	15.0	.0262
2	150	25	15.0	1.3	17.0	.0878
2	100	25	15.0	1.3	15.0	.0330
2	150	10	15.0	1.3	15.0	.0244
2	150	0	15.0	1.3	15.0	.0201
2	150	-15	15.0	1.3	15.0	.0236
*2	150	30	15.0	1.3	15.0	.0347
*2	150	30	10.0	1.3	15.0	.0271
*2	150	30	5.0	1.3	15.0	.0232
2	150	28	15.0	1.3	15.0	.0676
*2	150	25	15.0	1.3	15.0	.0327
2	150	22	15.0	1.3	15.0	.0289
*2	150	25	15.0	1.3	15.0	.0324
*,**2	150	25	15.0	1.3	15.0	-
*2	150	25	2.0	1.3	15.0	.0161
*2	150	20	15.0	1.3	15.0	.0282
2	150	31	15.0	1.3	15.0	.0732

TABLE V. - SWEPT MS(1)-317 ICING SPRAYS.

Á	V (mph)	TO (½F)	Ó (min.)	LWC (g/m^3)	MVD (μm)	C_d
*2	150	15	19.4	1.0	20.5	-
2	150	28	19.4	1.0	20.5	.05128
2	150	28	6.5	1.0	20.5	.02057
8	150	28	19.4	1.0	20.5	.05108
8	150	28	6.5	1.0	20.5	.02673
8	150	15	19.4	1.0	20.5	.03168
8	150	28	15.3	.26	12.0	.01520
*2	150	28	46.0	.26	12.0	-
2	150	15	6.5	1.0	20.5	.01475
2	150	0	6.5	1.0	20.5	.01377
**2	150	28	19.4	1.0	20.5	-
8	150	0	6.5	1.0	20.5	.01648
8	150	0	19.4	1.0	20.5	.02627
2	150	0	19.4	1.0	20.5	.01434
2	150	28	15.3	.26	12.0	.01170
2	150	28	19.4	1.0	20.5	.06865
2	150	0	46.0	.26	12.0	.01609

Note: Drag coefficients are based on chord length in free-stream direction (i.e. 3 feet). Drag coefficients were obtained for ice accretions at several angles-of-attack for all cases.

* Bad wake survey data.

** Ice shape mold taken. No drag data taken.

TABLE VI. - AIRFOIL IMPINGEMENT EFFICIENCY TESTS.

MODEL	α	V (mph)	MVD (μm)
NLF(1)-0414F	0	150	16.
"	0	150	20.
"	8	150	16.
"	8	150	20.
MS(1)-317	0	150	16.
"	0	150	20.
"	8	150	16.
"	8	150	20.
SWEPT MS(1)-317	0	150	16.
"	0	150	20.
"	8	150	16.
"	8	150	20.

TABLE VII. - PERCENT PERFORMANCE DEGRADATION FOR VARIOUS CASES.

Airfoil	α	V (mph)	TO (°F)	τ (min.)	LWC (g/m^3)	MVD (μm)	*$\%\Delta C_d$
NLF(1)-0414	0	150	28	15.0	1.0	20.5	486
"	0	150	28	5.0	1.0	20.5	106
"	0	150	0	15.0	1.0	20.5	83
"	0	150	0	5.0	1.0	20.5	47
"	6	150	28	15.0	1.0	20.5	261
"	6	150	28	5.0	1.0	20.5	74
"	6	150	0	15.0	1.0	20.5	74
"	6	150	0	5.0	1.0	20.5	46
MS(1)-317	2	150	31	15.0	1.3	15.0	510
"	2	150	25	5.0	1.3	15.0	100
"	2	150	5	15.0	1.3	15.0	68
"	2	150	5	5.0	1.3	15.0	27
"	6	150	25	15.0	1.3	15.0	181
Swept MS(1)-317	2	150	28	19.4	1.0	20.5	465
"	2	150	28	6.5	1.0	20.5	126
"	2	150	0	19.4	1.0	20.5	58
"	2	150	0	6.5	1.0	20.5	46
"	8	150	28	19.4	1.0	20.5	331
"	8	150	28	6.5	1.0	20.5	126
"	8	150	0	19.4	1.0	20.5	122
"	8	150	0	6.5	1.0	20.5	39

* $\%\Delta C_d = ((C_{d(iced)} - C_{d(clean)})/C_{d(clean)}) \times 100.$

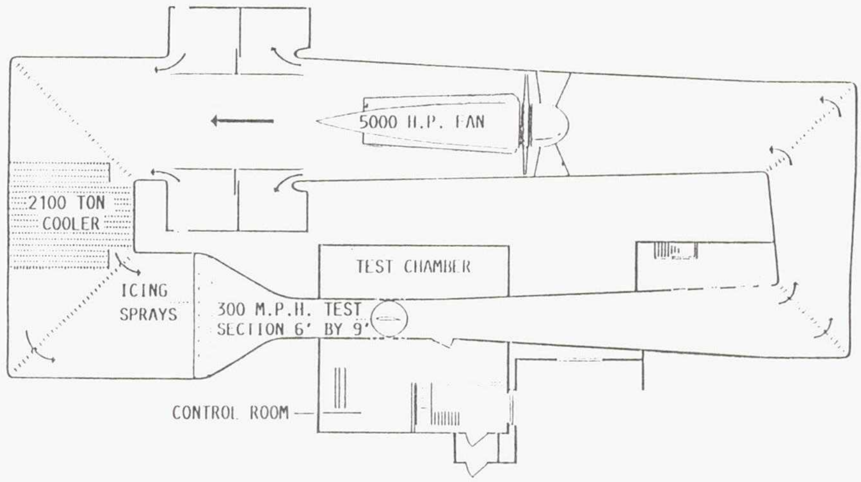

FIGURE 1. - NASA LEWIS ICING RESEARCH TUNNEL, PLAN VIEW.

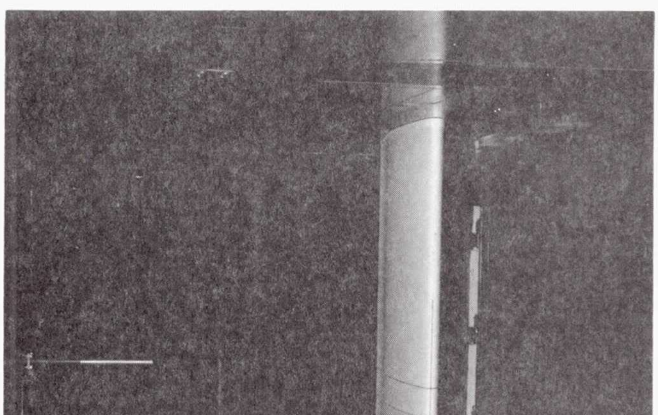

FIGURE 2. - INSTALLATION OF NLF(1)-0414 AIRFOIL IN ICING TUNNEL.

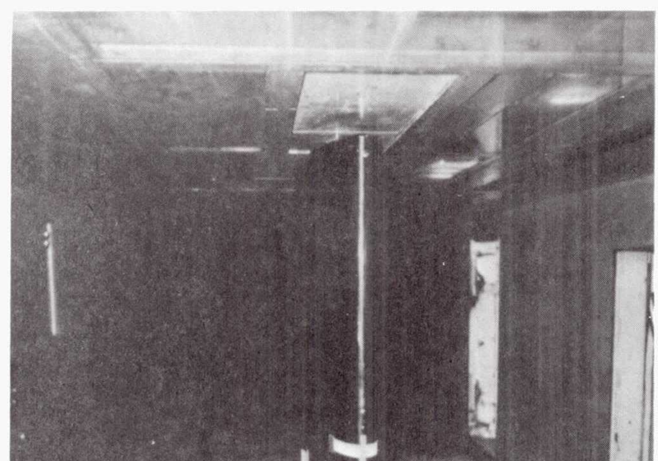

FIGURE 3. - INSTALLATION OF MS(1)-317 AIRFOIL IN TUNNEL SHOWING TYPICAL BLOTTER STRIP APPLICATION.

FIGURE 4. - INSTALLATION OF SWEPT MS(1)-317 AIRFOIL IN ICING TUNNEL.

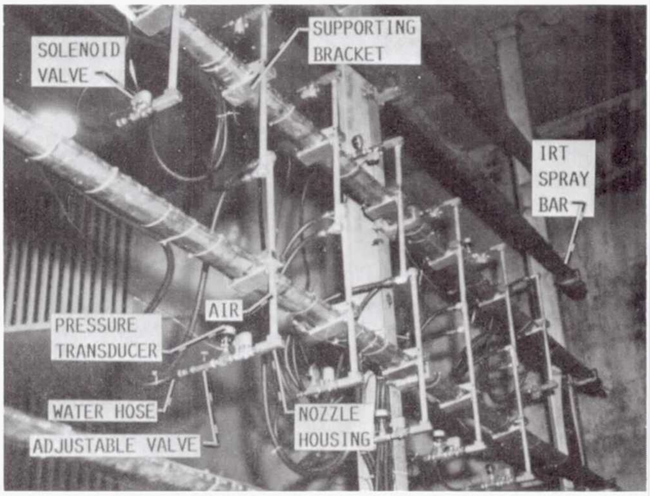

FIGURE 5. - INSTALLATION OF SPRAY NOZZLES FOR IMPINGEMENT TESTS.

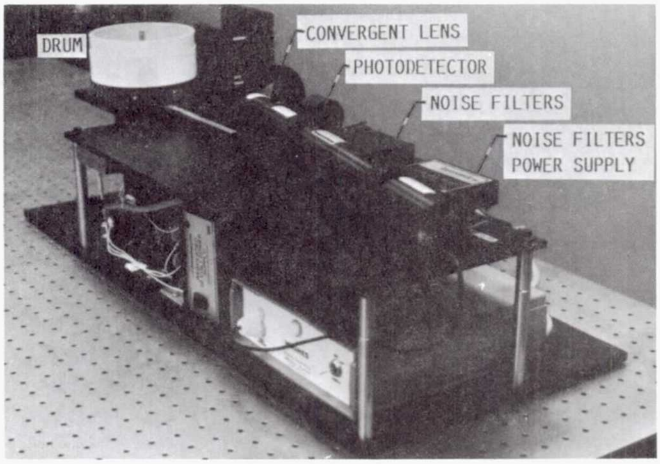

FIGURE 6. - AUTOMATED REFLECTOMETER USED TO REDUCE IMPINGEMENT DATA.

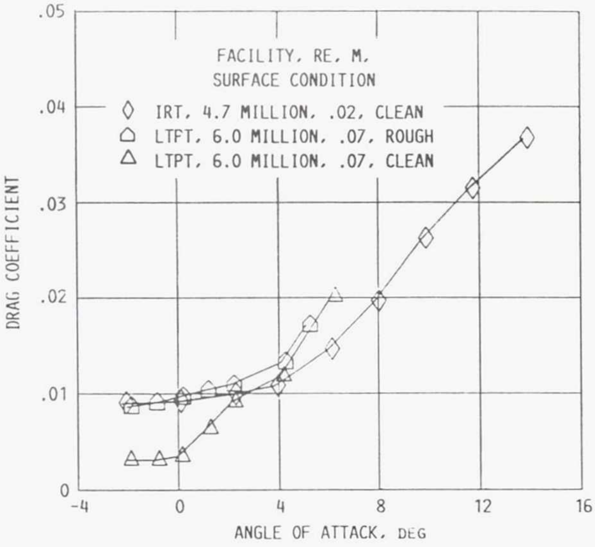

FIGURE 7. - DRAG COEFFICIENT FOR CLEAN NLF(1)-0414 AIRFOIL AS A FUNCTION OF ANGLE OF ATTACK.

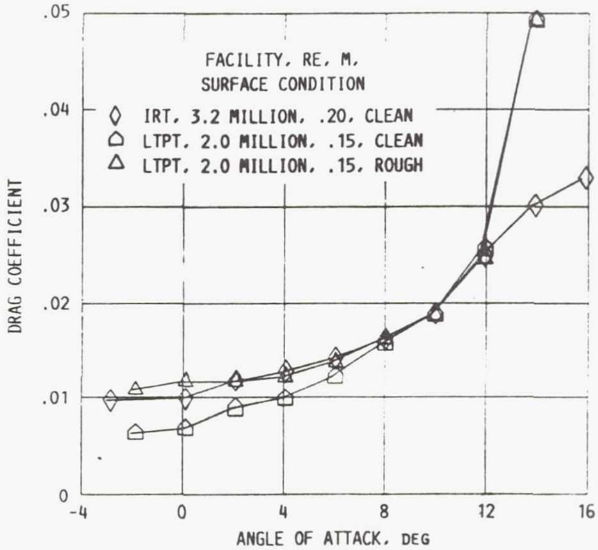

FIGURE 8. - DRAG COEFFICIENT FOR CLEAN MS(1)-317 AIRFOIL AS A FUNCTION OF ANGLE OF ATTACK.

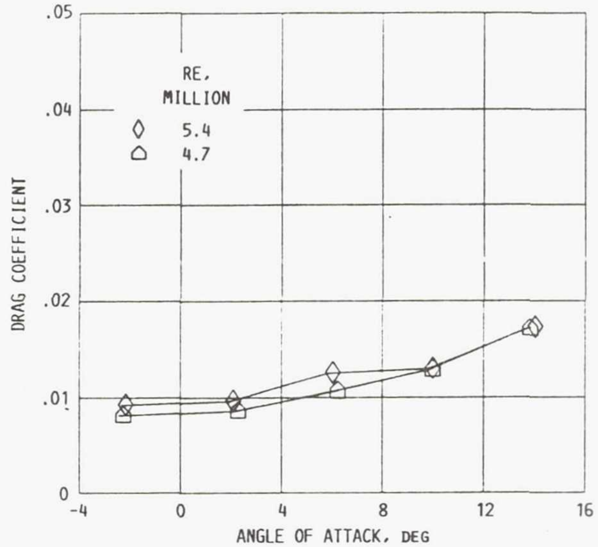

FIGURE 9. - DRAG COEFFICIENT FOR CLEAN SWEPT MS(1)-317 AIRFOIL AS A FUNCTION OF ANGLE OF ATTACK.

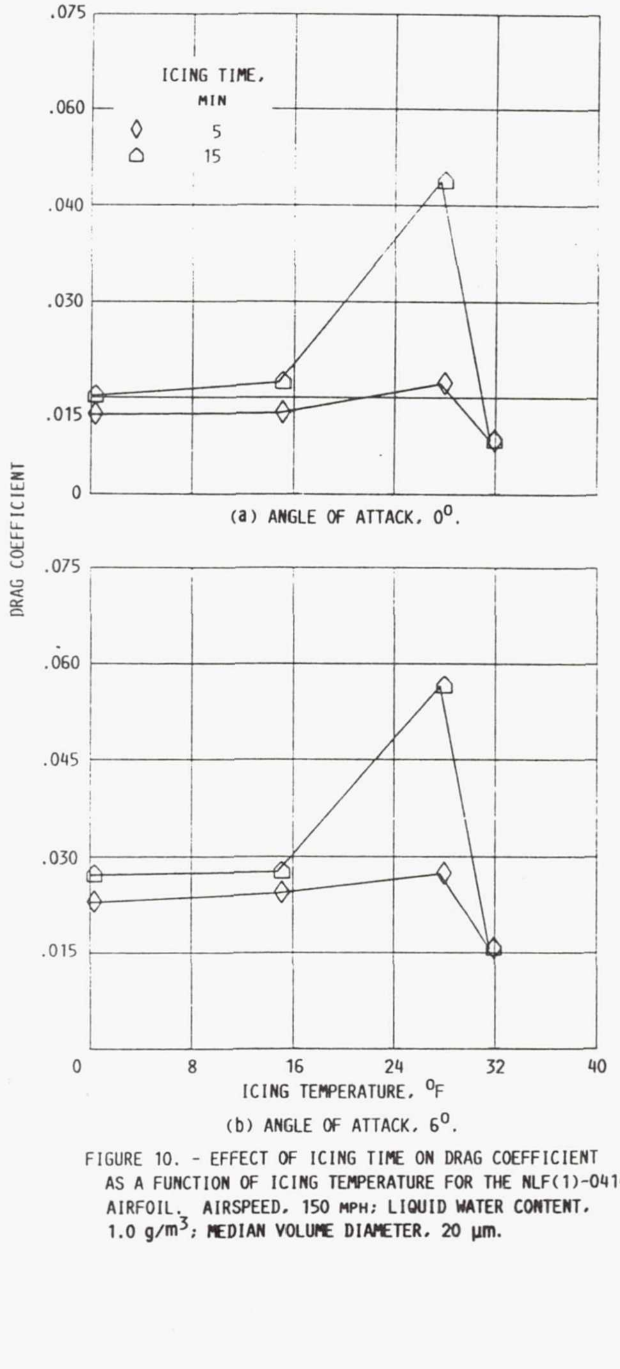

(b) ANGLE OF ATTACK, 6°.

FIGURE 10. - EFFECT OF ICING TIME ON DRAG COEFFICIENT AS A FUNCTION OF ICING TEMPERATURE FOR THE NLF(1)-0414 AIRFOIL. AIRSPEED, 150 MPH; LIQUID WATER CONTENT, 1.0 g/m^3; MEDIAN VOLUME DIAMETER, 20 μm.

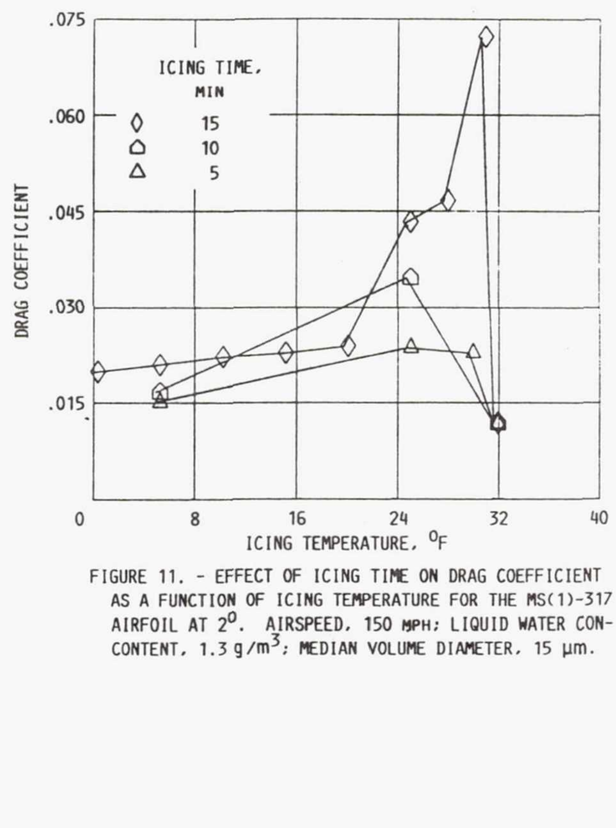

FIGURE 11. - EFFECT OF ICING TIME ON DRAG COEFFICIENT AS A FUNCTION OF ICING TEMPERATURE FOR THE MS(1)-317 AIRFOIL AT 2°. AIRSPEED, 150 MPH; LIQUID WATER CON-CONTENT, 1.3 g/m^3; MEDIAN VOLUME DIAMETER, 15 μm.

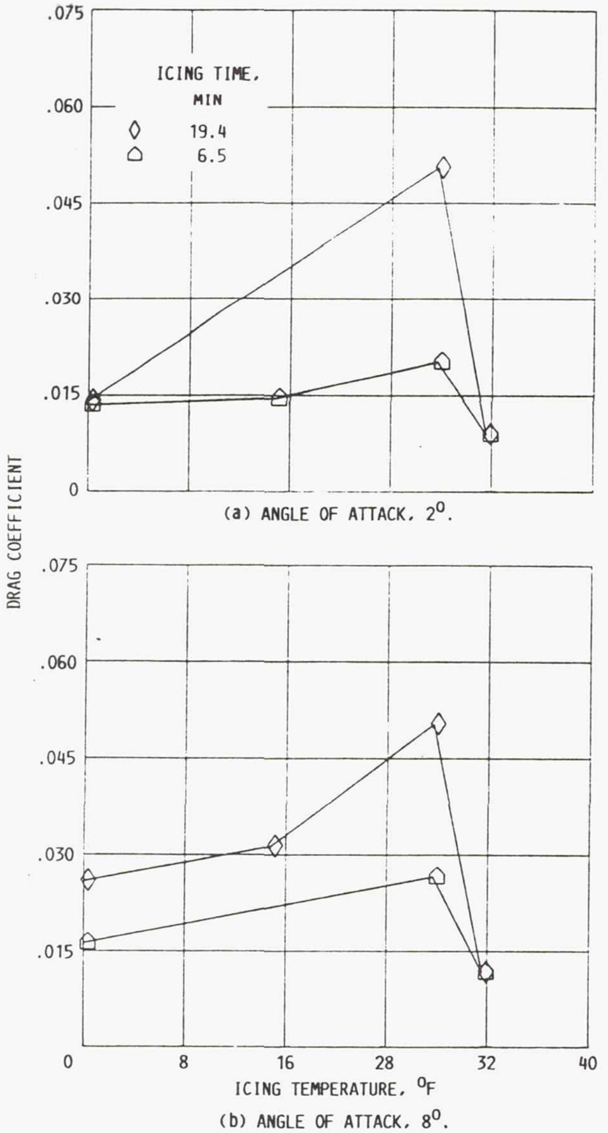

FIGURE 12. - EFFECT OF ICING TIME ON DRAG COEFFICIENT AS A FUNCTION OF ICING TEMPERATURE FOR THE SWEPT MS(1) -317 AIRFOIL. AIRSPEED, 150 MPH; LIQUID WATER CONTENT, 1.0 g/m^3; MEDIAN VOLUME DIAMETER, 20 μm.

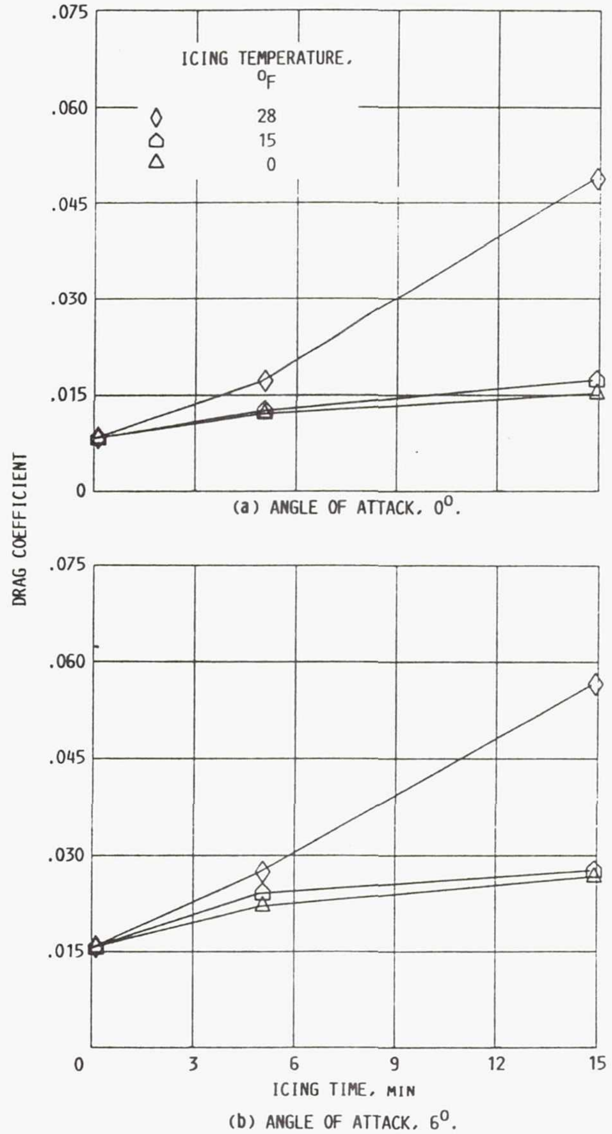

FIGURE 13. - EFFECT OF ICING TEMPERATURE ON DRAG COEFFICIENT AS A FUNCTION OF TIME IN ICING SPRAY FOR THE NLF(1)-0414 AIRFOIL. AIRSPEED, 150 MPH; LIQUID WATER CONTENT, 1.0 g/m^3; MEDIAN VOLUME DIAMTER, 20 μm.

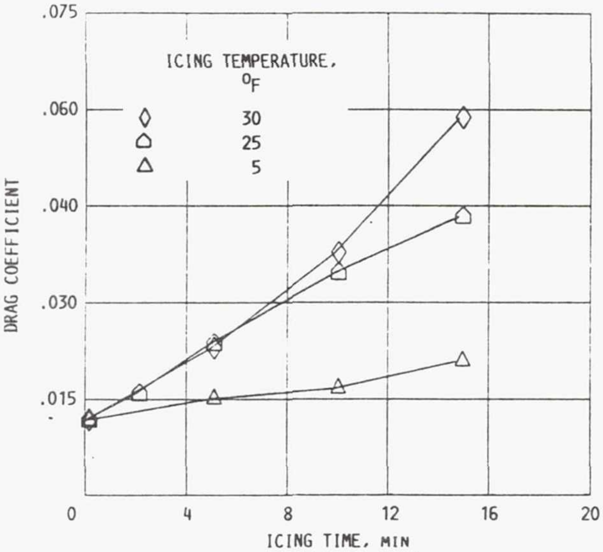

FIGURE 14. - EFFECT OF ICING TEMPERATURE ON DRAG COEFFICIENT AS A FUNCTION OF TIME IN ICING SPRAY FOR THE MS(1)-317 AIRFOIL AT 2°. AIRSPEED, 150 MPH; LIQUID WATER CONTENT, 1.3 g/m^3; MEDIUM VOLUME DIAMETER, 15 μm.

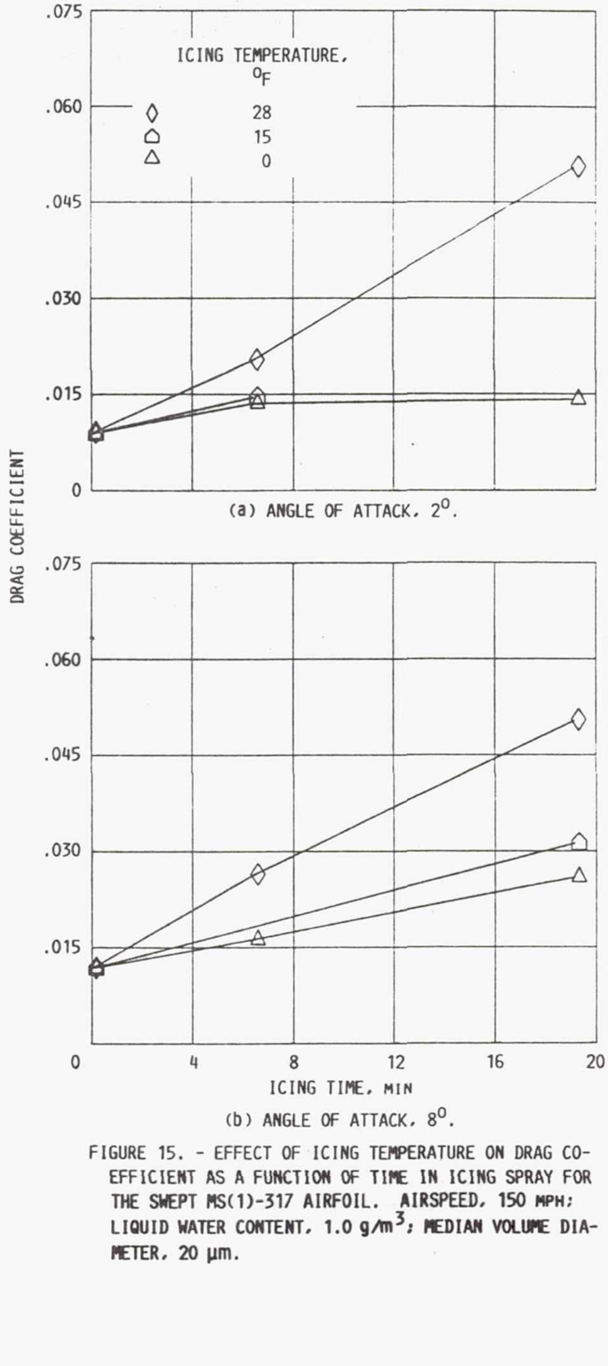

FIGURE 15. - EFFECT OF ICING TEMPERATURE ON DRAG COEFFICIENT AS A FUNCTION OF TIME IN ICING SPRAY FOR THE SWEPT MS(1)-317 AIRFOIL. AIRSPEED, 150 MPH; LIQUID WATER CONTENT, 1.0 g/m^3; MEDIAN VOLUME DIAMETER, 20 μm.

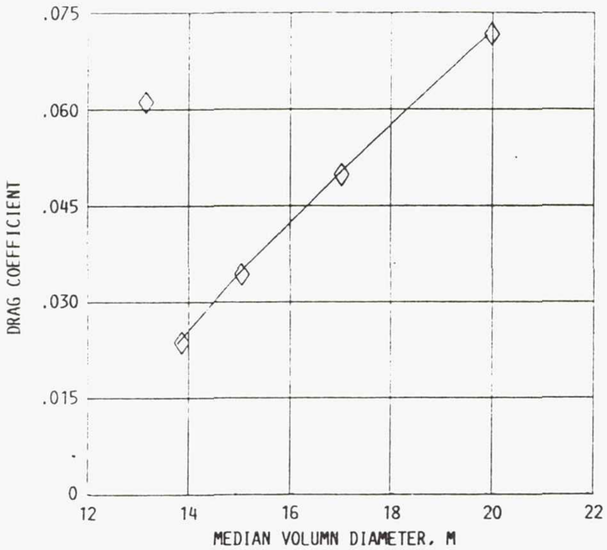

FIGURE 16. - DRAG COEFFICIENT AS A FUNCTION OF DROP SIZE FOR THE MS(1)-317 AIRFOIL AT 2°. AIRSPEED, 150 MPH; DATUM AIR TEMPERATURE, 25 °F; LIQUID WATER CONTENT, 1.3 g/m³.

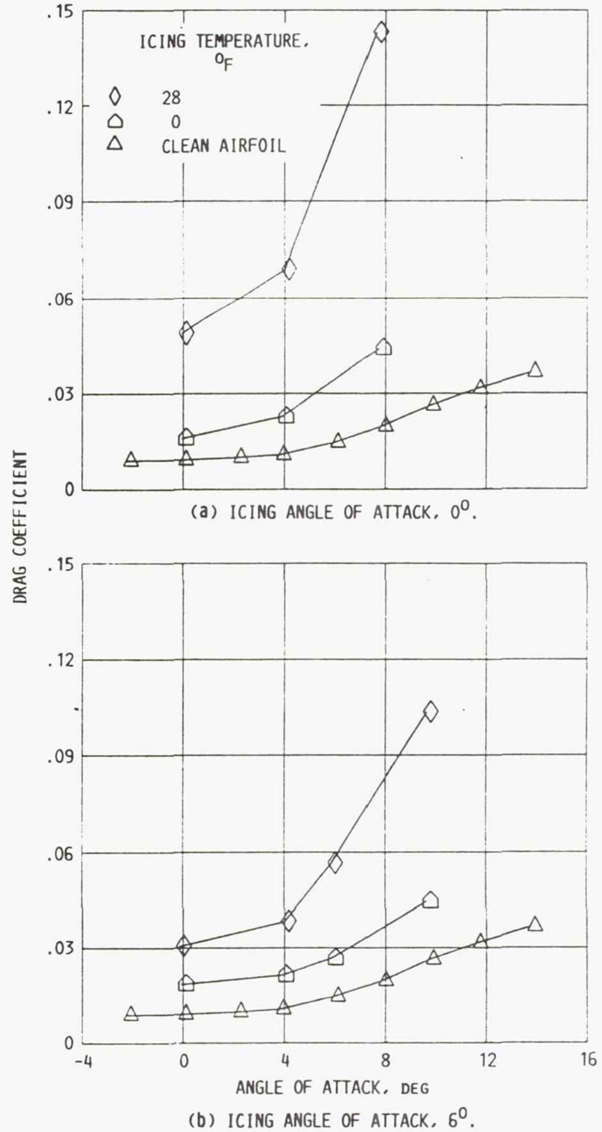

FIGURE 17. - EFFECT OF ICING TEMPERATURE ON DRAG COEFFICIENT AS A FUNCTION OF ANGLE OF ATTACK FOR THE ICED NLF(1)-0414 AIRFOIL. ICING CONDITIONS: AIRSPEED, 150 MPH; ICING TIME, 15.0 MINUTES; LIQUID WATER CONTENT, 1.0 g/m³; MEDIAN VOLUME DIAMETER, 20 μm.

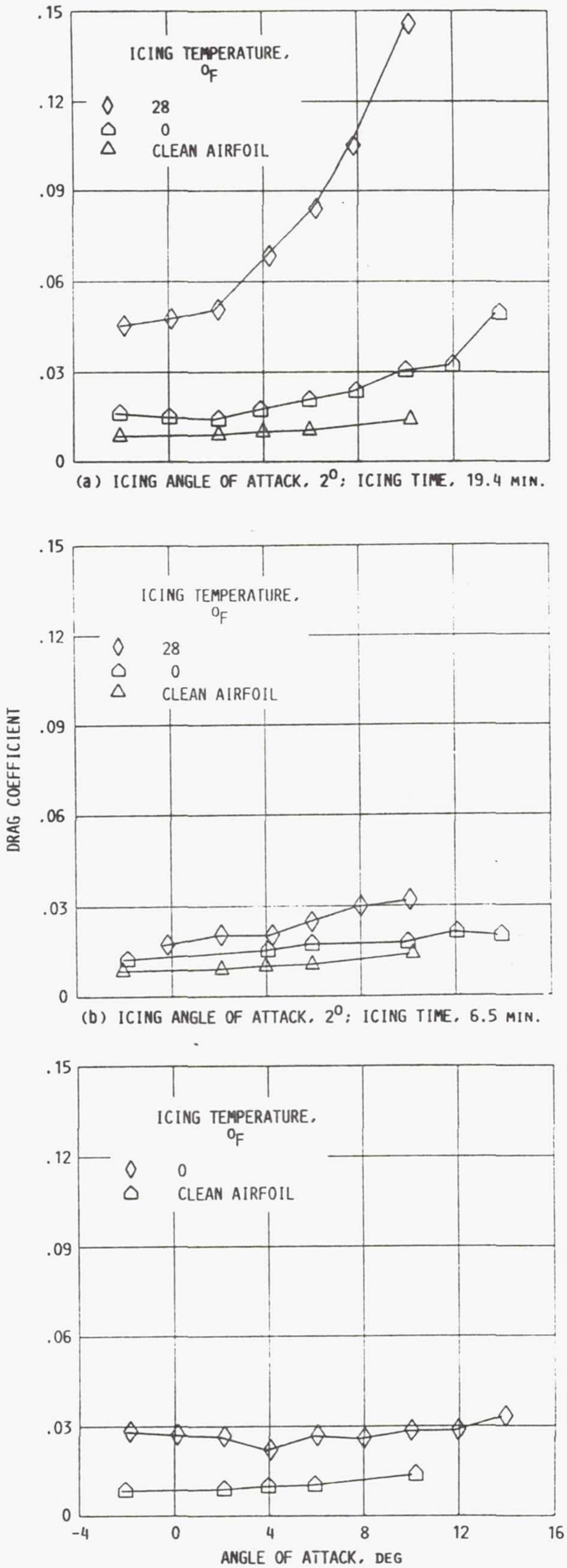

FIGURE 18. - EFFECT OF ICING TEMPERATURE ON DRAG COEFFICIENT AS A FUNCTION OF ANGLE OF ATTACK FOR THE ICED SWEPT MS(1)-317 AIRFOIL. ICING CONDITIONS; AIRSPEED, 150 MPH; LIQUID WATER CONTENT, 1.0 g/m^3; MEDIAN VOLUME DIAMETER, 20 µm.

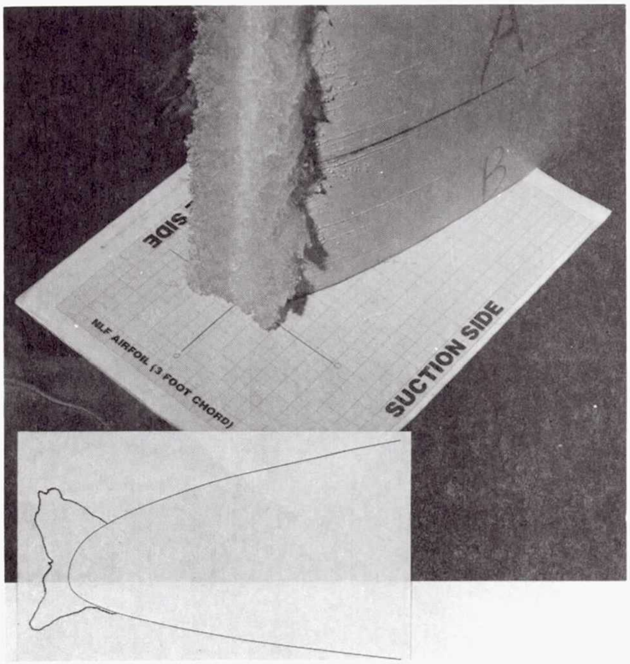

(a) PHOTOGRAPH AND TRACING. ICING ANGLE OF ATTACK, 0°; DATUM AIR TEMPERATURE, 28 $^{\circ}$F.

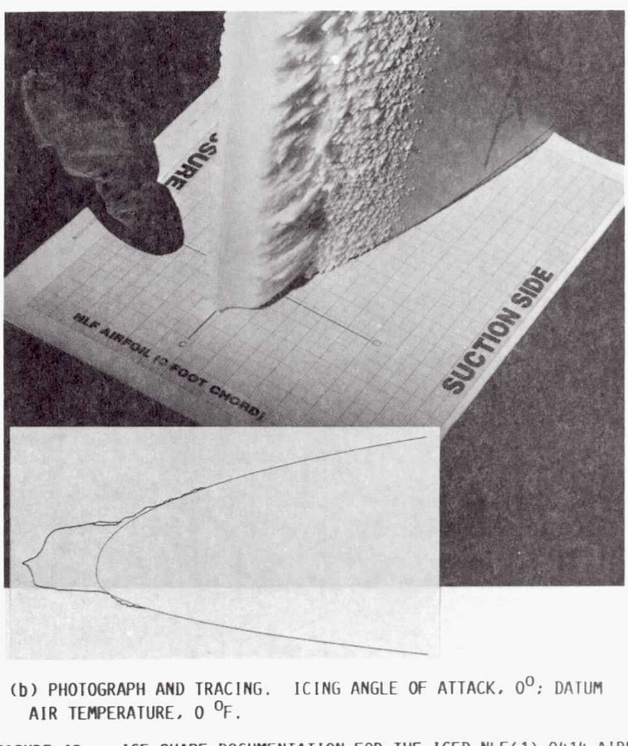

(b) PHOTOGRAPH AND TRACING. ICING ANGLE OF ATTACK, 0°; DATUM AIR TEMPERATURE, 0 $^{\circ}$F.

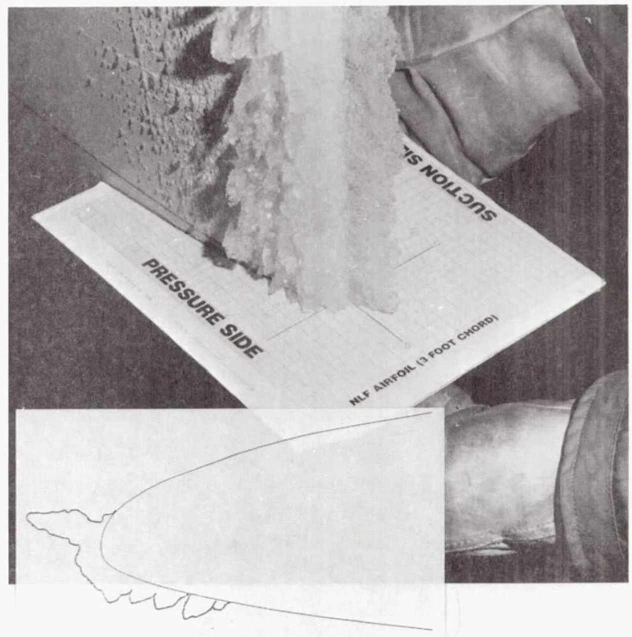

(c) PHOTOGRAPH AND TRACING. ICING ANGLE OF ATTACK, 6°; DATUM AIR TEMPERATURE, 28 $^{\circ}$F.

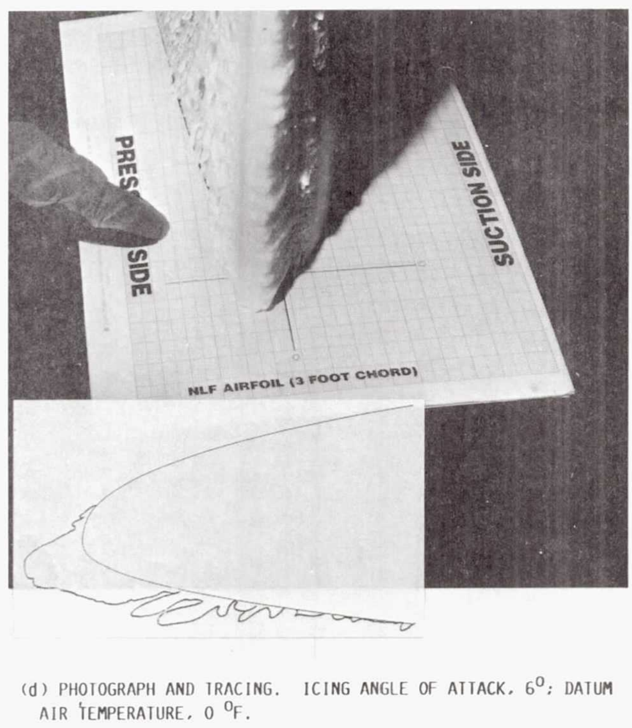

(d) PHOTOGRAPH AND TRACING. ICING ANGLE OF ATTACK, 6°; DATUM AIR TEMPERATURE, 0 $^{\circ}$F.

FIGURE 19. - ICE SHAPE DOCUMENTATION FOR THE ICED NLF(1)-0414 AIRFOIL. ICING CONDITIONS; AIRSPEED, 150 MPH; ICING TIME, 15.0 MINUTES, LIQUID WATER CONTENT, 1.0 g/m^3 MEDIAN VOLUME DIAMETER, 20 µm.

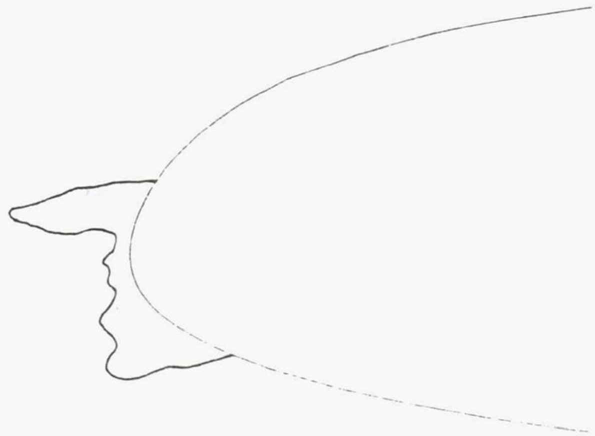

(a) ICING ANGLE OF ATTACK, 2^{o}; DATUM AIR TEMPERATURE, 25 ^{o}F.

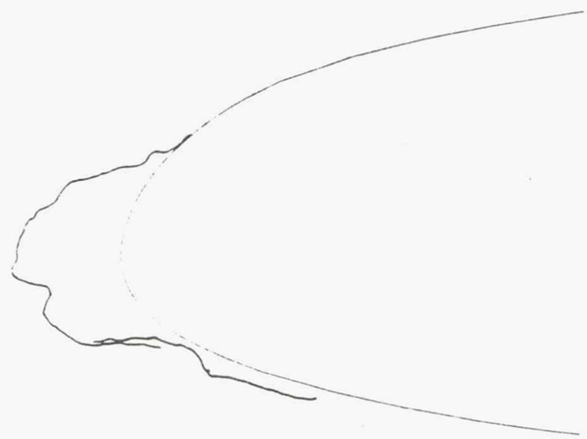

(b) ICING ANGLE OF ATTACK, 2^{o}; DATUM AIR TEMPERATURE, 0 ^{o}F.

ANGLE OF ATTACK, DEG

(c) ICING ANGLE OF ATTACK, 8^{o}; DATUM AIR TEMPERATURE, 28 ^{o}F.

FIGURE 20. - ICE SHAPE TRACINGS FOR THE ICED MS(1)-317 AIRFOIL. ICING CONDITIONS; AIRSPEED, 150 MPH; ICING TIME, 15.0 MINUTES; LIQUID WATER CONTENT, 1.3 g/m^3;

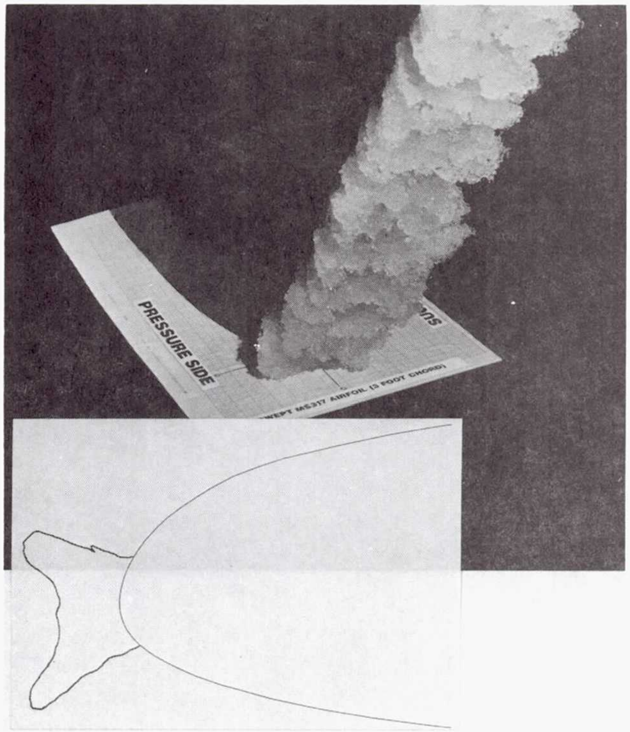

(a) PHOTOGRAPH AND TRACING. ICING ANGLE OF ATTACK, 2^{0}; DATUM AIR TEMPERATURE, 28 ^{0}F.

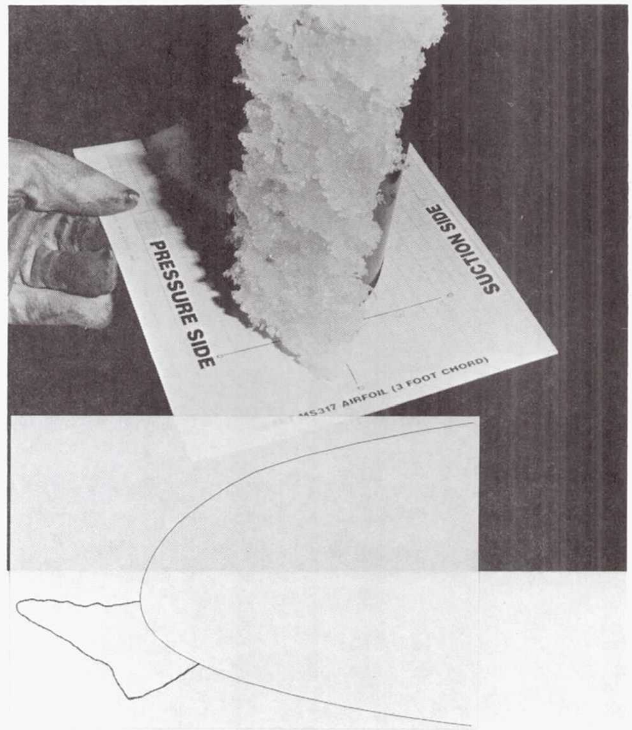

(c) PHOTOGRAPH AND TRACING. ICING ANGLE OF ATTACK, 8^{0}; DATUM AIR TEMPERATURE, 28 ^{0}F.

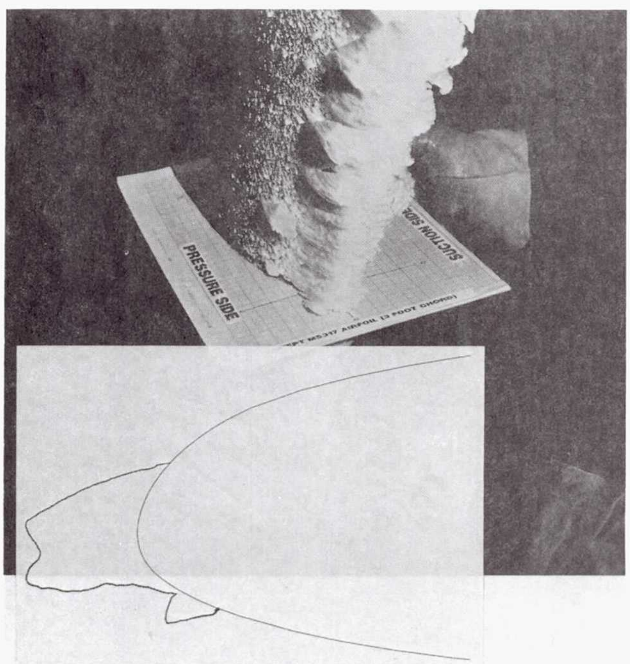

(b) PHOTOGRAPH AND TRACING. ICING ANGLE OF ATTACK, 2^{0}; DATUM AIR TEMPERATURE, 0 ^{0}F.

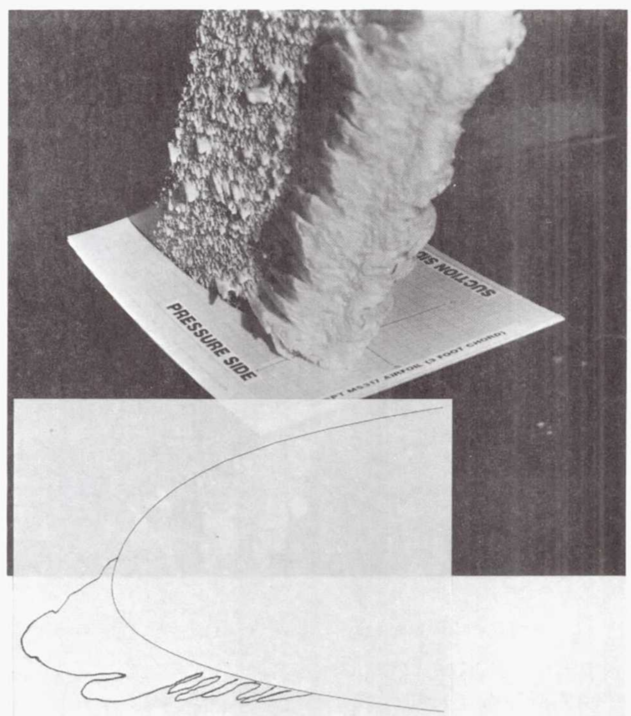

(d) PHOTOGRAPH AND TRACING. ICING ANGLE OF ATTACK, 8^{0}; DATUM AIR TEMPERATURE, 0 ^{0}F.

FIGURE 21. - ICE SHAPE DOCUMENTATION FOR THE ICED SWEPT MS(1)-317 AIRFOIL. ICING CONDITIONS: AIRSPEED, 150 MPH; ICING TIME, 19.4 MINUTES; LIQUID WATER CONTENT, 1.0 g/m^{3}; MEDIAN VOLUME DIAMETER, 20 µm.

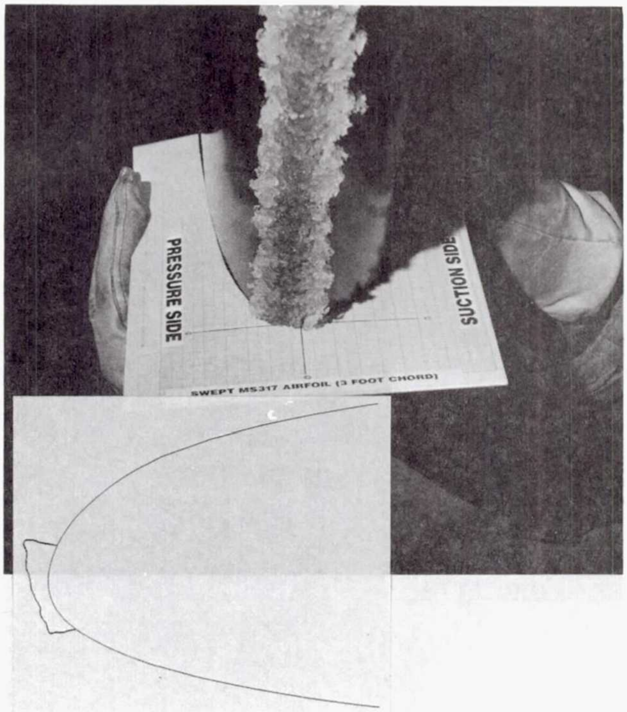

(a) PHOTOGRAPH AND TRACING. ICING ANGLE OF ATTACK, 2^{o}; DATUM AIR TEMPERATURE 28 ^{o}F.

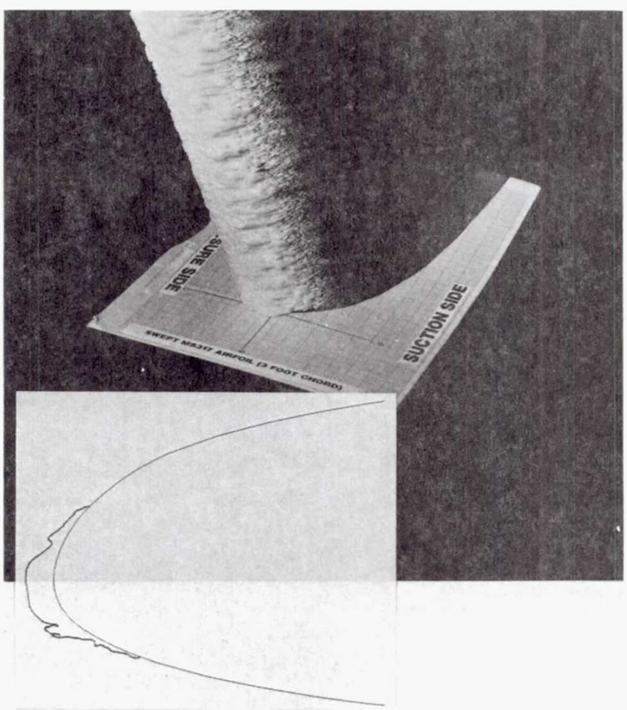

(b) PHOTOGRAPH AND TRACING. ICING ANGLE OF ATTACK, 2^{o}; DATUM AIR TEMPERATURE, 0 ^{o}F.

FIGURE 22. - ICE SHAPE DOCUMENTATION FOR THE ICED SWEPT MS(1)-317 AIRFOIL. ICING CONDITIONS; AIRSPEED, 150 MPH; ICING TIME, 6.5 MINUTES; LIQUID WATER CONTENT, 1.0 g/m^3; MEDIAN VOLUME DIAMETER, 20 μm.

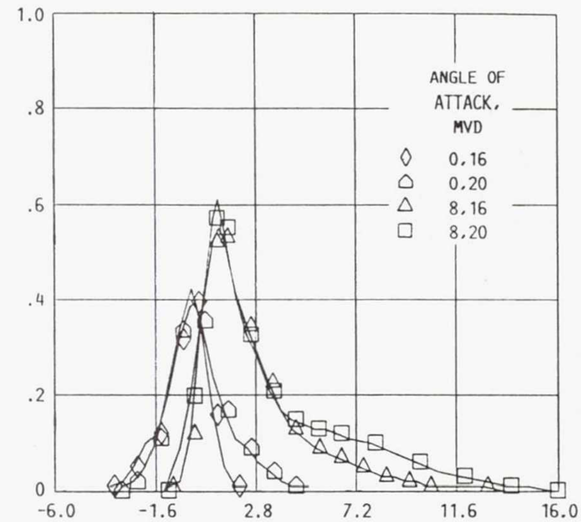

(a) NLF(1)-0414 AIRFOIL.

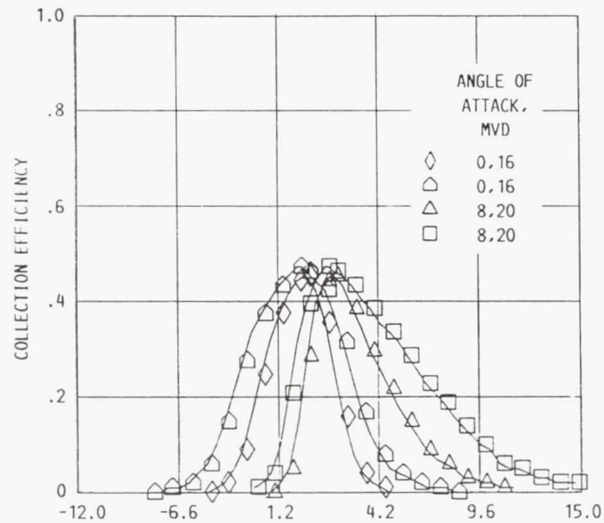

(b) MS(1)-317 AIRFOIL.

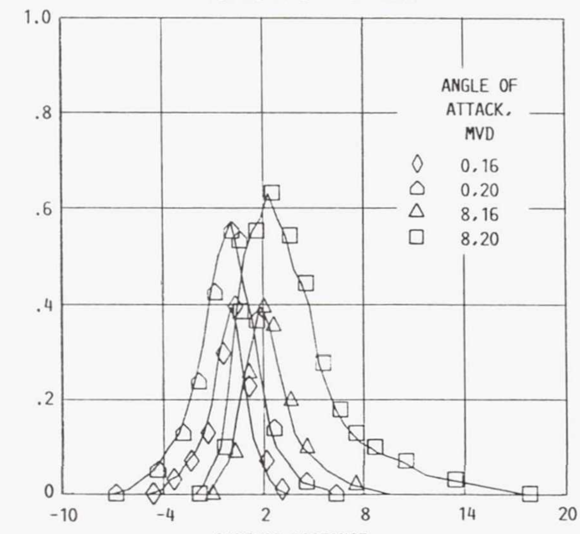

(c) SWEPT MS(1)-317 AIRFOIL.

FIGURE 23. - EFFECT OF ANGLE OF ATTACK AND DROP SIZE ON COLLECTION EFFICIENCY AS A FUNCTION OF SURFACE DISTANCE FROM THE HIGHLIGHT. AIRSPEED, 150 MPH; DATUM AIR TEMPERATURE; 40 ^{o}F.

NASA
National Aeronautics and Space Administration

Report Documentation Page

1. Report No.	2. Government Accession No.	3. Recipient's Catalog No.
NASA TM-103693 AIAA 91-0447		

4. Title and Subtitle	5. Report Date
Icing Characteristics of a Natural-Laminar-Flow, a Medium-Speed, and a Swept, Medium-Speed Airfoil	
	6. Performing Organization Code
7. Author(s)	8. Performing Organization Report No.
Colin S. Bidwell	E-5912
	10. Work Unit No.
	505-68-10
9. Performing Organization Name and Address	11. Contract or Grant No.
National Aeronautics and Space Administration Lewis Research Center Cleveland, Ohio 44135-3191	
	13. Type of Report and Period Covered
12. Sponsoring Agency Name and Address	Technical Memorandum
National Aeronautics and Space Administration Washington, D.C. 20546-0001	14. Sponsoring Agency Code

15. Supplementary Notes

Prepared for the 29th Aerospace Sciences Meeting sponsored by the American Institute of Aeronautics and Astronautics, Reno, Nevada, January 7-10,1991. Responsible person, Colin S. Bidwell (513) 433-3947.

16. Abstract

Tests were conducted in the Icing Research Tunnel at the NASA Lewis Research Center to determine the icing characteristics of three modern airfoils, a natural-laminar-flow, a medium-speed and a swept-medium-speed airfoil. The tests measured the impingement characteristics and drag degradation for angles-of-attack typifying cruise and climb for cloud conditions typifying the range that might be encountered in flight. The maximum degradation occurred for the cruise angle-of-attack for the long, glaze ice condition for all three airfoils with increases over baseline drag being 486%, 510%, and 465% for the natural-laminar-flow, the medium-speed and the swept; medium-speed airfoil respectively. For the climb angle-of-attack the maximum drag degradation (and extent of impingment) observed were also for the long, glaze ice condition and were 261%, 181% and 331% respectively. The minimum drag degradation (and extent of impingement) occurred for the cruise condition and for the short, rime spray with increases over baseline drag values of 47%, 28%, 46%, respectively.

17. Key Words (Suggested by Author(s))	18. Distribution Statement
Aircraft icing; Iced airfoil performance; Airfoil performance; Laminar flow airfoils; Medium-speed airfoils; Airfoil impingement efficiency	Unclassified – Unlimited Subject Category 02

19. Security Classif. (of this report)	20. Security Classif. (of this page)	21. No. of pages	22. Price*
Unclassified	Unclassified	32	A03

NASA FORM 1626 OCT 86

*For sale by the National Technical Information Service, Springfield, Virginia 22161